Astro2020 Science White Paper

Spatially Resolved Observations of the Ultraviolet Attenuation Curve

Thematic Areas: ☐ Planetary Systems ☒ Star and Planet Formation
☐ Formation and Evolution of Compact Objects ☐ Cosmology and Fundamental Physics
☐ Stars and Stellar Evolution ☐ Resolved Stellar Populations and their Environments
☒ Galaxy Evolution ☐ Multi-Messenger Astronomy and Astrophysics

Principal Author:
Name: Lea Hagen
Institution: Space Telescope Science Institute
Email: lhagen@stsci.edu
Phone: 667-218-6527

Co-authors: (names and institutions)

Benne W. Holwerda (University of Louisville)
Joanna Bridge (University of Louisville)
Alice Jacques (University of Louisville)
Bill Keel (University of Alabama)
Varsha Kulkarni (University of South Carolina)
Amanda Moffett (Vanderbilt University)
Julia Roman-Duval (Space Telescope Science Institute)

Abstract
Attenuation curves, which describe the effect of dust on unresolved stellar emission, are a combination of dust-star geometry and dust composition. Characterizing the ultraviolet (UV) attenuation curve, both for resolved and unresolved galaxies, is critical for our understanding of both the stellar populations and the dust content of galaxies over time. How dust affects our observations of the earliest galaxies remains poorly constrained despite local analog galaxy populations. We discuss two methods that can be used to observationally constrain the UV attenuation curve: spatially resolved spectral energy distribution modeling and overlapping galaxies. For these applications, UV observations with high spatial resolution ($<0.1''$) and some spectral information is key.

1 The Importance of Attenuation Curves

1.1 Introduction

To begin, it is necessary to distinguish between attenuation and extinction curves: they are qualitatively different, even though they are often used interchangeably in the literature. Often, the attenuation curve literature references both common extinction curves (e.g., Cardelli et al. 1989; Pei 1992; Misselt et al. 1999; Gordon et al. 2003) and attenuation curves (e.g., Calzetti et al. 1994, 2000). While these curves have been measured for a variety of locations and physical conditions, they trace fundamentally different physical processes.

An extinction curve is defined along one line of sight (generally to a star), and includes the effects of dust absorption and scattering out of the line of sight. Extinction curves can be used to directly infer the properties of dust grains (e.g., Draine 2003). An attenuation curve, on the other hand, represents the differences between a stellar population with and without dust. It includes the effects of dust absorption and scattered light (both into and out of the line of sight), and it is highly dependent on the geometry of stars and dust and on the star formation history (Kong et al. 2004; Buat et al. 2012; Reddy et al. 2010). There has been much discussion of the radiative transfer processes underlying the difference between attenuation and extinction curves (e.g., Witt & Gordon 2000; Wild et al. 2011; Calzetti 2013; Chevallard et al. 2013; Seon & Draine 2016; Narayanan et al. 2018), and relating the extinction and attenuation curves requires an assumption about the system geometry.

Attenuation curves have considerable variation. A selection of attenuation curves, normalized to a V-band (550 nm) attenuation of 1 magnitude, are plotted in Figure 1. At optical wavelengths, the curves predict nearly identical attenuations, but in the UV, they are quite different: both the slope and the absorption "bump" at 2175 Å (Stecher 1965) vary among the curves. At high redshift ($z \gtrsim 0.5$), where the UV is redshifted into the optical, there have been many measurements of the UV attenuation curve (e.g., Motta et al. 2002; York et al. 2006; Elíasdóttir et al. 2009; Perley et al. 2011; Kulkarni et al. 2011; Buat et al. 2012; Khare et al. 2012; Kriek & Conroy 2013; Scoville et al. 2015; Zeimann et al. 2015; Salmon et al. 2016). Large galaxy samples at lower redshift ($z \lesssim 0.2$) have used UV data from GALEX (e.g., Conroy et al. 2010; Wild et al. 2011; Battisti et al. 2016, 2017b,a; Leja et al. 2017; Salim et al. 2018), though its two filters only put weak constraints on the 2175 Å bump. Many of those studies, both at high and low redshift, have found correlations between the shape of the attenuation curve and galaxy properties like stellar mass and specific star formation rate (e.g., Conroy et al. 2010; Wild et al. 2011; Buat et al. 2012; Kriek & Conroy 2013; Zeimann et al. 2015; Salmon et al. 2016; Leja et al. 2017; Battisti et al. 2017a; Tress et al. 2018; Salim et al. 2018). Within nearby galaxies, spatially resolved variations have been found in the shape of attenuation curve as well (Roussel et al. 2005; Calzetti et al. 2005; Hoversten et al. 2011; Dong et al. 2014; Hutton et al. 2015; Hagen et al. 2017; Hagen et al. 2019, *submitted*). Radiative transfer modeling also suggests that variation should be present (e.g., Witt & Gordon 2000; Wild et al. 2011; Calzetti 2013; Chevallard et al. 2013; Seon & Draine 2016; Narayanan et al. 2018).

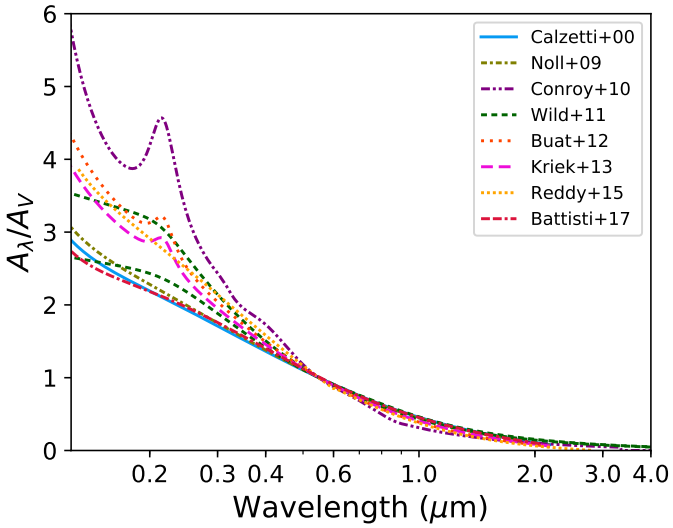

Figure 1: A selection of attenuation curves measured for a variety of galaxy samples across a range of redshifts. Individually, each of these curves also represent a range of measured slopes and 2175 Å bump strengths. In the next decade, we will need high resolution UV imaging to constrain the variation of the attenuation curve with respect to dust and galaxy properties.

1.2 Inferring Intrinsic Luminosities

Rest-frame UV light is commonly used as an indicator of recent ($\sim$100 Myr) star formation (e.g., Kennicutt 1998) in both nearby and distant galaxies. However, UV light is efficiently absorbed by dust, so analysis requires a correction for any dust. To make this correction, one utilizes an attenuation curve, which describes the combined effects of absorption and scattering at every wavelength.

As an example of the significance of this correction, one could imagine a typical star-forming galaxy. Far-UV (FUV) flux is commonly used to calculate the recent star formation rate (SFR) of a galaxy (e.g., Hao et al. 2011), especially at intermediate redshift, where rest-frame FUV can easily be observed from the ground; in the era of JWST, FUV will be a star formation tracer through the epoch of reionization. If one wishes to find the dust-corrected FUV flux, the attenuation curves in Figure 1 at 1500 Å give a wide range of possible A_λ/A_V values. For a galaxy with a fairly typical A_V of 0.5, this represents a variation of a factor of 2.4 in the dust-corrected flux value, and therefore the inferred SFR.

1.3 Deriving Dust and ISM Properties

Since the attenuation curve traces a combination of dust grain properties and dust-star geometry, radiative transfer (RT) modeling can be used to simultaneously reveal both attenuation and geometry, and therefore constrain the dust properties. This has been done on a limited scale for local galaxies (e.g., De Looze et al. 2012, 2014; Viaene et al. 2017), but the current state-of-the-art requires several assumptions, including the spatial distribution of stars and dust, which make it difficult to match the observed UV fluxes. Since the UV encodes important information about dust properties, the continued development of RT codes will improve the return on UV data. In addition, once RT modeling has been broadly tested and its results confirmed in local galaxies, it can be confidently used in high-redshift unresolved galaxies to constrain the earliest growth and structure of dust.

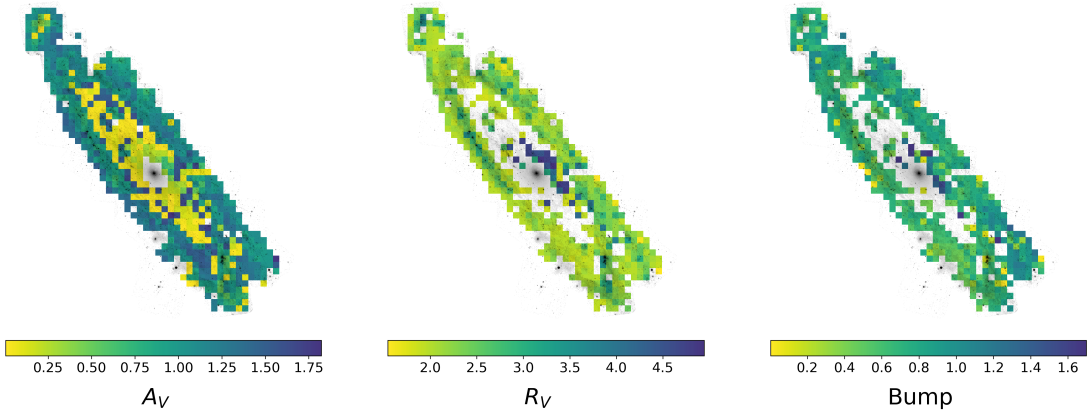

Figure 2: Maps of the attenuation curve shape in M31, inferred using UV to near-IR SED fitting of 500 pc pixels (Hagen et al. 2019, *submitted*). Maps like these across a range of galaxy properties, including high-redshift analogs, will enable better constraints of star formation and dust properties at high redshift.

2 Research Strategies

In this section, we discuss approaches to measuring the UV attenuation curve that will grow the field over the next decade. In particular, we assert that spatially resolved measurements over a variety of galaxy metallicities, morphologies, and environments will have a large impact on our understanding of the ISM and star formation in both the local and high-redshift universe.

2.1 Spatially Resolved SED Modeling

Modeling the spectral energy distributions (SEDs) of galaxies is a common tool for inferring physical parameters like stellar mass, age, and dust content. More recently, with advances in model sophistication and computational techniques, SED modeling has been used for components of galaxies to create maps of their physical properties. While this has far-reaching implications for galaxy evolution, we focus on its potential for understanding attenuation curves and dust.

In Figure 2, we show recent results from Hagen et al. (2019, *submitted*), which undertook SED modeling of pixels in M31, in which the attenuation curve slope and 2175 Å bump strength were included as free parameters. This technique promises to reveal variations in the attenuation curve shape and how that variation relates to small-scale galaxy properties. Applying this to large samples of galaxies will point to changes in dust geometry, dust grain properties, and how best to interpret the SEDs of unresolved galaxies.

2.2 Overlapping Galaxy Pairs

To study dust inside different kinds of galaxies, overlapping or occulting galaxy pairs are eminently suited. Unlike Herschel observations, the occulting galaxy technique does not suffer from source confusion and it can confidently measure zero extinction, ruling out dust at certain locations within or near a galaxy. The number of overlapping pairs of galaxies has steadily risen

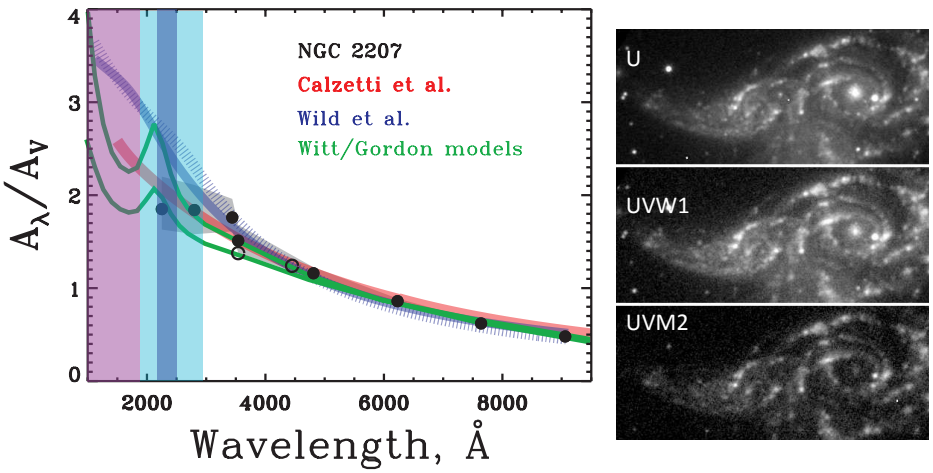

Figure 3: The attenuation curve (left) for the interacting and backlit galaxy NGC 2207 (right) based on GALEX-Optical-Spitzer data (Keel et al. 2014). Their single attenuation curve (points) is most consistent with a Calzetti relation. (Calzetti & Heckman 1999; Wild et al. 2009) not the Milky Way's. Ideally UV filters would map the characteristic bump in the Milky Way Curve (green line) with a narrow band on the feature (dark blue) and broad NUV/FUV filters (light blue/purple) to characterize the curve.

to several thousand[1] (Keel et al. 2013; Holwerda et al. 2015) and the shape and dependencies of the attenuation curve on location within galaxies or on galaxy population traits can now be tackled.

While the total dust attenuation (e.g., A_V) can be inferred from single filter images, the attenuation curve needs multi-color observations or spectroscopy (Figure 3). Multiple broad-band filters (e.g., Holwerda et al. 2009; Keel et al. 2014) can reveal the attenuation curve measured over areas limited by distance and image quality. Alternatively, integral field unit (IFU) observations can be used to map the attenuation curves in overlapping galaxy pairs. Pilot IFU observations (Holwerda et al. 2013; Holwerda & Keel 2013, Jacques et al. *in prep*) already reveal a variety of attenuation curves using just optical wavelengths. IFU observations are limited by field-of-view and spatial resolution. The optimal case would be a MUSE-like instrument on a 8-meter class telescope available to the US community. Wavelength coverage and spatial resolution are critical to resolve the attenuation relation in nearby overlapping galaxy pairs. In case of multi-wavelength observations, high-resolution ($\sim$1$''$) ultraviolet imaging is critical to resolve the 2175 Å bump in the attenuation law (Figure 3).

Observatories such as Hubble (see Jacques+ *in prep*), Swift, AstroSat, and the proposed CASTOR, can certainly play a role in providing a wide-filter ultraviolet observation in addition to the optical and near-infrared information on attenuation curves from overlapping galaxies. However, to constrain the distinguishing feature in the attenuation curve at 2100 Å, one critically

[1]With the advent of LSST, galaxy blends are closer to the norm than the exception and the number of bona fide overlapping galaxies is expected to rise in turn.

needs either spectroscopy (ultraviolet, preferably IFU) or narrow-band ultraviolet imaging capability with high spatial resolution.

2.3 High-Redshift Analog Populations

As an example of the unresolved stellar populations for which attenuation curves are very much needed, Luminous Blue Spheroids (LBSs) are a possible high-redshift analog population of compact, round-looking blue spheroidal galaxies (Kelvin et al. 2014). In contrast to the apparently rare appearance of such galaxies in previous studies, LBSs appear to become more common at the low masses probed by current deep redshift surveys. Moffett et al. (2016) found that LBS galaxies make up 11.5% of a $r < 19.8$ and $z < 0.06$ GAMA galaxy sample or $\sim$15-20% of the $M_* < 10^9 M_\odot$ population, implying that these galaxies are a decidedly non-trivial evolutionary path for low-mass galaxies.

LBS galaxies represent plausible downsized (lower mass and more recently formed) analogues of the high-redshift "blue nuggets," believed to form through a process of gas compaction triggered by mergers or significant gas accretion (Barro et al. 2013; Dekel & Mandelker 2014; Zolotov et al. 2014, e.g.,). do all blue nuggets quench into red nuggets and grow into low-redshift ellipticals, or do some grow disks and form the core of low-redshift disk galaxies ((as suggested by Graham et al. 2015)? A better map of their dust properties (distribution, attenuation curves) would then serve to better understand the high-redshift population to which they are analogous.

3 Observational Requirements

In order to move UV attenuation curve work into the next decade and beyond, we need to create statistical samples of spatially resolved UV attenuation curves across a wide range of galaxy properties. In order to probe a sufficient variety of rare types, including high-redshift analogs, we need UV galaxy observations out to $\sim$500 Mpc ($z\sim$0.1). Star-forming regions are generally $<$250 pc across (Pleuss et al. 2000), so resolving down to that physical scale requires a spatial resolution of 0.1$''$ or better.

The wavelength coverage should be at least as blue as 1000 Å to ensure good far-UV measurements shortward of the 2175 Å bump. A range of medium- or narrow-band filters would enable strong constraints on both the slope and bump strength. An IFU or two-axis grism observations (to act as an IFU-like cube) would provide additional information on the precise shape of the attenuation curve and any variation in the width of the bump.

References

Barro, G., Faber, S. M., Perez-Gonzalez, P. G., et al. 2013, ArXiv e-prints

Battisti, A. J., Calzetti, D., & Chary, R.-R. 2016, ApJ, 818, 13

—. 2017a, ApJ, 851, 90

—. 2017b, ApJ, 840, 109

Buat, V., Noll, S., Burgarella, D., et al. 2012, A&A, 545, A141

Calzetti, D. 2013, Star Formation Rate Indicators, ed. J. Falcón-Barroso & J. H. Knapen (Cambridge University Press), 419

Calzetti, D., Armus, L., Bohlin, R. C., et al. 2000, ApJ, 533, 682

Calzetti, D., & Heckman, T. M. 1999, ApJ, 519, 27

Calzetti, D., Kinney, A. L., & Storchi-Bergmann, T. 1994, ApJ, 429, 582

Calzetti, D., Kennicutt, Jr., R. C., Bianchi, L., et al. 2005, ApJ, 633, 871

Cardelli, J. A., Clayton, G. C., & Mathis, J. S. 1989, ApJ, 345, 245

Chevallard, J., Charlot, S., Wandelt, B., & Wild, V. 2013, MNRAS, 432, 2061

Conroy, C., Schiminovich, D., & Blanton, M. R. 2010, ApJ, 718, 184

De Looze, I., Baes, M., Fritz, J., & Verstappen, J. 2012, MNRAS, 419, 895

De Looze, I., Fritz, J., Baes, M., et al. 2014, A&A, 571, A69

Dekel, A., & Mandelker, N. 2014, MNRAS, 444, 2071

Dong, H., Li, Z., Wang, Q. D., et al. 2014, ApJ, 785, 136

Draine, B. T. 2003, ARA&A, 41, 241

Elíasdóttir, Á., Fynbo, J. P. U., Hjorth, J., et al. 2009, ApJ, 697, 1725

Gordon, K. D., Clayton, G. C., Misselt, K. A., Landolt, A. U., & Wolff, M. J. 2003, ApJ, 594, 279

Graham, M. L., Sand, D. J., Zaritsky, D., & Pritchet, C. J. 2015, ArXiv e-prints

Hagen, L. M. Z., Siegel, M. H., Hoversten, E. A., et al. 2017, MNRAS, 466, 4540

Hao, C.-N., Kennicutt, R. C., Johnson, B. D., et al. 2011, ApJ, 741, 124

Holwerda, B. W., Böker, T., Dalcanton, J. J., Keel, W. C., & de Jong, R. S. 2013, MNRAS, 433, 47

Holwerda, B. W., & Keel, W. C. 2013, A&A, 556, A42

Holwerda, B. W., Keel, W. C., Williams, B., Dalcanton, J. J., & de Jong, R. S. 2009, AJ, 137, 3000

Holwerda, B. W., Reynolds, A., Smith, M., & Kraan-Korteweg, R. C. 2015, MNRAS, 446, 3768

Hoversten, E. A., Gronwall, C., Vanden Berk, D. E., et al. 2011, AJ, 141, 205

Hutton, S., Ferreras, I., & Yershov, V. 2015, MNRAS, 452, 1412

Keel, W. C., Manning, A. M., Holwerda, B. W., Lintott, C. J., & Schawinski, K. 2014, AJ, 147, 44

Keel, W. C., Manning, A. M., Holwerda, B. W., et al. 2013, PASP, 125, 2

Kelvin, L. S., Driver, S. P., Robotham, A. S. G., et al. 2014, MNRAS, 439, 1245

Kennicutt, Jr., R. C. 1998, ARA&A, 36, 189

Khare, P., Vanden Berk, D., York, D. G., Lundgren, B., & Kulkarni, V. P. 2012, MNRAS, 419, 1028

Kong, X., Charlot, S., Brinchmann, J., & Fall, S. M. 2004, MNRAS, 349, 769

Kriek, M., & Conroy, C. 2013, ApJ, 775, L16

Kulkarni, V. P., Torres-Garcia, L. M., Som, D., et al. 2011, ApJ, 726, 14

Leja, J., Johnson, B. D., Conroy, C., van Dokkum, P. G., & Byler, N. 2017, ApJ, 837, 170

Misselt, K. A., Clayton, G. C., & Gordon, K. D. 1999, ApJ, 515, 128

Moffett, A. J., Ingarfield, S. A., Driver, S. P., et al. 2016, MNRAS, 457, 1308

Motta, V., Mediavilla, E., Muñoz, J. A., et al. 2002, ApJ, 574, 719

Narayanan, D., Conroy, C., Dave, R., Johnson, B., & Popping, G. 2018, ArXiv e-prints

Pei, Y. C. 1992, ApJ, 395, 130

Perley, D. A., Morgan, A. N., Updike, A., et al. 2011, AJ, 141, 36

Pleuss, P. O., Heller, C. H., & Fricke, K. J. 2000, A&A, 361, 913

Reddy, N. A., Erb, D. K., Pettini, M., Steidel, C. C., & Shapley, A. E. 2010, ApJ, 712, 1070

Roussel, H., Gil de Paz, A., Seibert, M., et al. 2005, ApJ, 632, 227

Salim, S., Boquien, M., & Lee, J. C. 2018, ApJ, 859, 11

Salmon, B., Papovich, C., Long, J., et al. 2016, ApJ, 827, 20

Scoville, N., Faisst, A., Capak, P., et al. 2015, ApJ, 800, 108

Seon, K.-I., & Draine, B. T. 2016, ApJ, 833, 201

Stecher, T. P. 1965, ApJ, 142, 1683

Tress, M., Mármol-Queraltó, E., Ferreras, I., et al. 2018, MNRAS, 475, 2363

Viaene, S., Baes, M., Tamm, A., et al. 2017, A&A, 599, A64

Wild, V., Charlot, S., Brinchmann, J., et al. 2011, MNRAS, 417, 1760

Wild, V., Walcher, C. J., & Johansson, P. H. 2009, ArXiv e-prints

Witt, A. N., & Gordon, K. D. 2000, ApJ, 528, 799

York, D. G., Khare, P., Vanden Berk, D., et al. 2006, MNRAS, 367, 945

Zeimann, G. R., Ciardullo, R., Gronwall, C., et al. 2015, ApJ, 814, 162

Zolotov, A., Dekel, A., Mandelker, N., et al. 2014, ArXiv e-prints